# Breakup and coalescence of drops during transition from dripping to jetting in a Newtonian fluid

VISWANATHAN, Harish

# Breakup and Coalescence of Drops during Transition from Dripping to Jetting in a Newtonian Fluid

H. Viswanathan*

*Department of Engineering and Mathematics, Sheffield Hallam University, Howard Street, Sheffield, England, S1 1WB, United Kingdom*

## ABSTRACT

We present numerical simulations of dripping to jetting transitions that occur during the flow of a Newtonian liquid. An axis-symmetric, Volume of Fluid (VOF) model along with Continuum Surface Force (CSF) representation is developed to capture various regimes of drop formation. By numerically studying different nozzle diameters subjected to various flow rates, we examine the critical conditions under which the dripping to jetting transition takes place. At every stage of dripping and jetting, we assess the accuracy of the present simulations through a number of comparisons with previously published experimental data and empirical correlation and find reasonable agreements. Our numerical simulations show different responses that characterize the dripping and the dripping faucet regimes leading to chaotic dripping patterns. Within the chaotic regime, we identify four unique modes of satellite formation and their merging patterns which have not been reported earlier. Finally, we observe that as soon as the flow rate approaches a threshold the jetting regime begins where, subsequent disintegration of drops and coalescence patterns are observed downstream. Detailed flow patterns, pressure distributions and drop shapes are provided for various dimensionless numbers alongside the spatial-temporal resolutions of both jetting and coalescence of primary drops. Of the many complex dynamics that influence the primary droplet coalescence, we find that the oscillatory motion of drops during their travel downstream, which is dampened normally due to viscous effects, can be influential and can aid both coalescence and breakup of droplets.

*Keywords*: Dripping to Jetting; Chaotic Dripping response; VOF; Coalescence of drops; Numerical Simulation; Satellite drop formation.

**Highlights**

- Axis-symmetric numerical simulations for predicting dripping to jetting transitions for a Newtonian fluid using the VOF model.
- Model results agree well with previously published experimental results and correlations for periodic dripping, dripping faucet and jet breakup lengths.
- New modes of satellite formation and merging with primary drops during chaotic dripping are identified.
- Prediction of coalescence of primary drops downstream during jetting.

***Corresponding author information:** Email: h.viswanathan@shu.ac.uk ; Phone: +0441142256244

## 1. Introduction

Drop formation from nozzle finds its application in various fields such as ink-jet printing, encapsulation, food engineering and chemical synthesis. Over the centuries, researchers have studied various factors that partake in the breakup of drops in Newtonian liquids for different regimes realizing its importance to controlling those parameters to attain the desired goals. Several investigations have been carried out theoretically, experimentally and more recently, the advancements in computational techniques and high-performance computing have led to undertaking detailed numerical simulations for investigating droplet break-up mechanisms at various levels. The experimental studies on drop formation that have evolved for over centuries, paid significant attention to three regimes of drop formation namely, a) *periodic dripping* (*PD*), b) *dripping faucet* (*DF*) and c) *jetting* (*J*) that occur at incremental values of Weber number (*We*) when the flow rate reaches a threshold value. Many researchers have studied the (*PD*) regime (Tate, 1864; Rayleigh, 1899) that occurs at $We<<1$, for understanding how surface tension forces to gravitational forces played a vital role in drop detachment and associated mass of pendant drop (Harkins and Brown, 1919).

Experimental investigations have shown that the pendant drop proceeds through a range of profiles until a critical volume is reached when part of the drop detaches itself (Pitts, 1976). Zhang and Basaran (1995) reported the time evolution of drops and presented the images of a liquid thread that connects the bottom portion of the drop that is about to detach from the rest of the liquid that is pendant from the tube. It was also shown that the breakup of liquid threads could potentially lead to the formation of satellite drops at much smaller flow rates. The increase in *We* leads to (*DF*) regime, which is an intermediary regime where period doubling, chaos and hysteresis are observed (Sartorelli et. al., 1994; Coullet et. al., 2005). With further increase in *We*, (*J*) regime (Savart, 1833; Plateau, 1873; Rayleigh, 1879) is observed where a continuous stream of liquid emanates from the nozzle and disintegrates into drops downstream at a distance greater than $10D$ for low viscosity fluids such as water. However, the transition from dripping to jetting (Ambravaneswaran et al., 2004; Subramani et. al., 2006) was experimentally studied by Clanet and Lasheras (1999) in detail, who provide a criterion for the transition to occur at a critical Weber number ($We_c$) which was shown to be a function of Bond numbers of the inside and outside diameters of the tube and *K*, an empirically obtained constant with a value of 0.37. Sallam et. al., (2002) reported several breakup modes for jets for varying *We* such as, a weakly turbulent Rayleigh-like breakup observed at small jet exit *We* and Reynolds numbers (*Re*), a turbulent breakup observed at moderate jet exit *We*, and an aerodynamic bag/shear breakup observed at large jet *We*. The investigations by Sallam et. al., (2002) led to the development of expressions for various modes of jet breakup length as a function of *We*.

From a numerical standpoint, pendant drop formation and breakup have successfully been investigated in the past addressing the nonlinearities associated with the pinch-off region (Subramani et. al., 2006; Davidson and Cooper-White; 2006; Notz et. al., 2001). Eggers and Dupont (1994) applied the one-dimensional (1D) slender jet approximations to Navier-Stokes equations using boundary element analysis whilst Chen et al. (2002) examined pinch-off and scaling during drop formation using two-dimensional (2D) finite element methods (FEM) for glycerol-water solutions. Using the 2D FEM, Notz et. al., (2001) have examined the formation of satellites at low flow rate dripping and predicted that a thin liquid thread was a precursor to satellite formation corroborating the findings from Zhang and Basaran (1995). Che et. al., (2011) investigated the breakup process of pendant drops using three-dimensional (3D) numerical simulation that was carried out using the Level Set Method (LSM). Their studies emphasized the effects of surface tension and the outer diameter of the capillary on the amplitude and the period of the pressure fluctuation of the drop during pinch-off. Laminar jetting in still air was studied by Pan and Suga (2006) using 3D LSM with Continuous Surface tension Force (CSF). Their studies showed that for jets featuring relatively high Ohnesorge number (*Oh*), the rearrangement of the axial velocity profile and surface shear induce initial large scale vortex structures inside the liquid core. The numerical simulations from Pan and Suga (2006) also showed that the violent breakup within the inside

of the jet is due to the large scale vortex motion which is amplified by surface instability when the energy of the jet is accumulated enough to overcome inertial and surface tension forces. By choosing the (VOF) model coupled with Large Eddy Simulations (LES) in 3D, Farvardin and Dolatabadi (2013) investigated jets from elliptical orifices for capturing primary breakup in Rayleigh regime. They numerically characterize the axis-switching phenomenon where the jet axis switches by changing the major and minor axis in a 90°shift. However, they reported that their numerical results were unable to capture satellite drop formation that was experimentally reported for jets at certain *We*. Delteil et. al., (2011) studied rounded jets using a one-fluid model coupled with VOF method to represent the jet break-up and numerically verifying that no parasitic currents effected the capillary forces. Their simulations were performed with water injection at 308 K in supercritical $CO_2$, show that the breakup length starts to increase until it stabilizes to a distance down which the fragmentation of the jet occurs. The core jet length variations have been reported in their simulations suggesting that once the jet is established, the droplet break-up length could potentially oscillate with time. In addition, they report critical findings from their numerical simulations that the first droplets generated by the jet breakup have a diameter below two-fold the jet diameter and as droplets move downstream, their numerical simulations showed a tendency to close their shape, catch-up and potentially coalesce. Their studies motivated to further our numerical investigations to understand downstream coalescence and catch-up of drops.

Numerically, modelling all the responses associated with transition from dripping to jetting have received significant attention owing to various reasons, but not limited to *i*) understanding drop formation, its shape and dynamics at different regimes, *ii*) to examine the interface capturing techniques' ability to predict such transient responses and *iii*) identification of new response periods of dripping and jetting. Rodríguez and Saborid, (2017) have recently demonstrated through a 1D numerical model based on the conservation form of the system of Differential-Algebraic equations (DAE) and computed both the linear stability analysis and the nonlinear transient behaviour of equilibrium solutions for capturing slender jets and examined the transitions. A rigorous 3D model was developed by Xiao et al., (2016) who studied the transition from dripping to jetting using a Coupled Level Set/Volume of Fluid (CLSVOF) technique adopted for interface-tracking coupled with Large Eddy Simulations (LES). The main focus of their study was to test and validate the CLSVOF-LES formulation in 3D to predict the three regimes namely, the (*PD*), (*DF*) and (*J*) under the same conditions experimented by Clanet and Lasheras (1999) with constant geometrical properties. In addition, they performed simulations with two additional *We* in higher jetting regimes with the same inlet diameter of the orifice. Their simulations characterized that the jet breakup length is linearly proportional with respect to liquid velocity. More recently, drop formation have been addressed by solving axis-symmetric Navier-Stokes equations coupled with CLSVOF have shown evidences of new dripping responses for high viscous fluids by Chakraborty et al.,(2016) moreover, such methods have also detailed the interface overturning features during breakup (Borthakur et. al., (2017)).

Previous axis-symmetric studies using CLFVOF methods (Chakraborty et al., 2016; Borthakur et. al., 2017) have shown to represent intricate details on dripping to jetting transitions as much as the previously reported 3D CLSVOF simulations (Xiao et al., 2016;) and 3D LSM (Pan and Suga (2006)). Although, the aforementioned studies on the axis-symmetric models as well as the full 3D simulations have focused on drop formation and break up extensively but have not detailed the downstream dynamics of drops such as oscillatory motion of drops and coalescence of primary drops in the (*J*) regime have not been reported previously neither in 2D nor with the 3D simulations. In the present study, we develop an axis-symmetric VOF model to numerically investigate the liquid's response to *We* by changing the flow rates (*Q*) and to explore the various regimes of drop formation in quiescent air. The advantage of VOF method is that it ensures mass conservation is intrinsically satisfied and representation of droplet coalescence is well predicted (Nikolopoulos et. al., 2009; Delteil et al., 2011). Additionally, VOF has also been investigated and validated previously for pinch-off behavior in pendant drops (Zhang, 1999; Davidson and Cooper-White; 2006) Our objective in the present study is twofold; a) to validate our model

predictions for transitions from (*PD*) to (*DF*) and then to (*J*) responses against the previously published experimental results from Clanet and Lasheras (1999) for various nozzle diameters and *We* and b) to elucidate the breakup patterns and the nonlinear dynamics of drop interactions that occur downstream in the aforementioned regimes. In addition, we will focus on the (*J*) regime to examine the disintegration of the jet length and its temporal variance, and its dependence on *We*. This is carried out by comparing the numerical predictions of the mean jet breakup length and experimental correlations derived by Sallam et. al., (2002).

## 2. Problem Statement

### *2.1. System details*

The system of interest is an axis-symmetric domain shown in Fig.1, represented by cylindrical coordinates ($r$, $z$), where $r$ is the radial coordinate and $z$ is the axial co-ordinate in the direction of gravity $\boldsymbol{g}$ respectively. The liquid, at a constant flow rate $Q$, that is injected from the nozzle is assumed to be incompressible and Newtonian with viscosity $\mu_w$ and density $\rho_w$ and the flow to be axis-symmetric, whose origin lies at the center of the open end of the nozzle. In the present study, we assume that the fluid from the nozzle of radius ($R$) is injected into an incompressible, quiescent air of viscosity $\mu_a$ and density $\rho_a$.

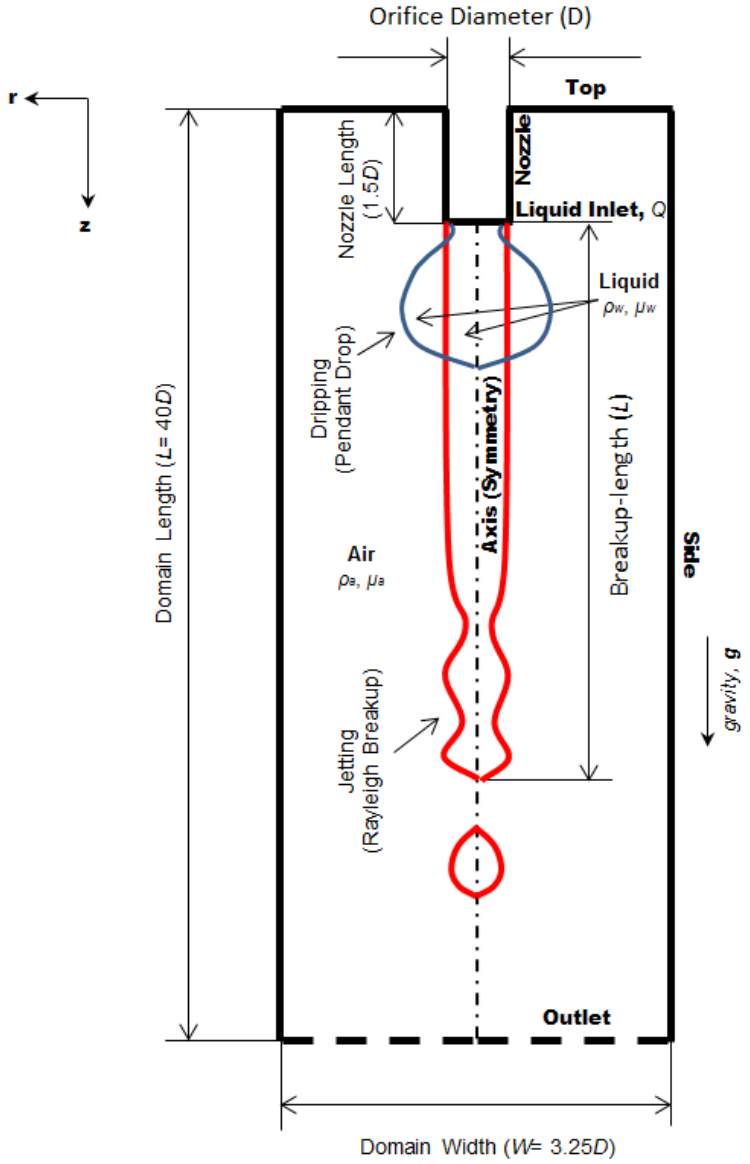


**Fig.1.** Schematic of an axis-symmetric domain showing droplet formation during various regimes of liquid flow at a constant inflow velocity.

The liquid-air interface has a constant surface tension $\sigma$ both spatially and temporally, and is free to deform. In the present work, only half of the jets and droplets are simulated by applying conditions of symmetry, purely to reduce the computational resource requirements.

| *Fluid* | *Density ($kg/m^3$)* | *Viscosity (Pa.s)* | *Air-Water Interfacial surface tension (N/m)* |
|---|---|---|---|
| *Water* | *1000* | *$10^{-3}$* | *0.0728* |
| *Air* | *1.22* | *$8.76 \times 10^{-5}$* | |

**Table.1.** Properties of fluids used in the present study.

For validation purposes, we study with fluid properties provided in Table.1 and with orifice radii of the nozzles provided in Table.2 that are consistent with experimental data from Clanet and Lasheras (1999).

| *Sc.no* | $D_0$ (mm) | $D$ (mm) | $D/D_0$ |
|---|---|---|---|
| *i* | *0.90* | *0.584* | *0.648* |
| *ii* | *1.66* | *1.20* | *0.727* |
| *iii* | *2.12* | *1.60* | *0.758* |
| *iv* | *2.78* | *2.156* | *0.778* |

**Table.2.** Orifice radii of nozzles used for investigation in the present numerical simulations.

The wall thickness of the tube is neglected in the present study as reviewed by several researchers (Zhang and Basaran, 1995; Zhang, 1999; Wikes et al.,1999) that global features of the dynamics such as drop length, volume and capillary breakup are virtually unaffected by the wall thickness ($D_0$) provided that $D/D_0 > 0.3$.

### *2.2. Governing equations*

The equations that describe the motion of both fluids that are incompressible and present within the system are represented by a single set of Navier-Stokes Equations given as follows:

The continuity equation is given as

$$\boldsymbol{\nabla} \cdot (\rho \vec{\boldsymbol{v}}) = 0 \qquad (1)$$

and the momentum equation is described by

$$\frac{\partial}{\partial t}(\rho \vec{\boldsymbol{v}}) + \boldsymbol{\nabla} \cdot (\rho \vec{\boldsymbol{v}} \vec{\boldsymbol{v}}) = -\nabla p + \boldsymbol{\nabla} \cdot [\mu(\boldsymbol{\nabla} \vec{\boldsymbol{v}} + \boldsymbol{\nabla} \vec{\boldsymbol{v}}^T)] + \rho \vec{\boldsymbol{g}} + \vec{\boldsymbol{F}} \qquad (2)$$

where $\vec{\boldsymbol{v}} = (u, v)$ is the velocity vector with components $u$ and $v$ that represent radial and axial components of the velocity field respectively. In the above equation, $p$ is the pressure $\vec{\boldsymbol{g}} = (0, g)$ is the gravitational acceleration and $t$ is the time. $\vec{\boldsymbol{F}}$ is the continuum surface tension force on the interface of the volume fraction field $\alpha$, given by

$$\vec{F} = \sigma k \nabla \alpha \quad (3)$$

where $k$ is the local curvature on the interface and is computed as

$$k = -\nabla \cdot \left(\frac{\nabla \alpha}{|\nabla \alpha|}\right) \quad (4)$$

In terms of describing the interface between immiscible fluids, namely, water and quiescent air and providing volume fraction conservation throughout the domain, two-phase flow using the Volume of Fluid method (VOF) is incorporated. The VOF equation is given by:

$$\frac{\partial \alpha}{\partial t} + \nabla \cdot (\alpha \vec{v}) = 0 \quad (5)$$

The volume fraction gives the portion of the cell which is filled with either phase, where

$\alpha = 0$ the cell is filled with air (the continuous fluid)
$0 < \alpha < 1$ the interface exists in the cell (6)
$\alpha = 1$ the cell is filled with liquid (the dispersed fluid, namely; water in this study)

The density $\rho$ and viscosity $\mu$ can be expressed as linear contributions from each phase as follows:

$$\rho = \rho_w \alpha + \rho_a (1 - \alpha) \quad (7)$$
$$\mu = \mu_w \alpha + \mu_a (1 - \alpha) \quad (8)$$

The following dimensionless numbers are used in this study to characterize dripping to jetting transition and for illustrating the jet break-up.

The Weber number ($We$) that relates the fluids inertia compared its surface tension and illustrates whether kinetic energy or the surface tension energy is dominant.

$$We = \frac{\rho_w {V_0}^2 D}{\sigma} \quad (9)$$

The Bond number ($Bo$) that characterizes the shape of droplets by relating gravitational force to surface tension force.

$$Bo = \frac{\rho_w g D^2}{\sigma} \quad (10)$$

The current study is limited to laminar jets where the Reynolds number is given by

$$Re = \frac{\rho_w V_0 D}{\mu} < 2300 \quad (11)$$

In the above Eqs. (9-11), $V_0$ is the mean velocity and is related to the volumetric flow rate of the liquid entering the tube, given by $Q = \pi D^2 V_0$. Although the outer diameter ($D_0$) is not used anywhere in our simulations, we provide this parameter only for scaling purposes and for consistent comparison with experimental data.

### *2.3. Boundary and Initial conditions*

In the domain of interest shown in Fig.1, a constant flow rate *Q* that corresponds to a mean velocity ($V_0$) was specified at the nozzle orifice pertaining to an inlet boundary condition. The symmetry or slip boundary condition was provided on the axis and a no-slip boundary condition at the top (wall) and nozzle was implemented. On the side, a free slip condition was used and at the outlet, a pressure-outlet boundary condition was used. On the free surface however, two conditions apply namely, *a)* a kinematic condition, that there should be no mass transfer across the free surface and *b)* a dynamic condition, that viscous and surface tension stresses should be in balance. To find the influence of the side and outlet boundaries, simulations were performed with different side widths ranging from 1.5*D* to 4.5*D* and outlets ranging from 10*D* to 40*D*. Typically, for lower *We* that comprise the (*PD*) and (*DF*) regimes, a domain width of 3.25*D* and length of 15*D* (Chakraborty et. al., 2016; Xiao et. al., 2016; Borthakur et. al., 2017) has no influence on the simulations and all events of interest are well predicted. However, for the (*J*) regime, a domain size between 40-80*R* was chosen to resolve the events of interest downstream. The domain was initialized with still air with properties at standard temperature and pressure conditions.

### *2.4. Numerical Solution Procedure*

The numerical simulations that are presented in the current study were performed using commercially available finite-volume based software package ANSYS Fluent (Version 18.0). The flow equations are solved using a laminar incompressible, transient model integrated with the VOF method (Hirt and Nichols, 1981) in explicit formulation using a double-precision solver. The pressure-velocity scheme used was PISO that splits the solution into predictor and corrector steps, alongside the Non-Iterative Algorithm (NITA) which provides faster convergence. The discretized moment equation was approximated using the QUICK scheme and the gradients of the scalars were computed by using the Least-Squares cell-based method. The Least-Squares cell-based was chosen since it is directly comparable to node-based gradient methods, much accurate compared to cell based methods and is computationally less intensive. The "PRESTO!" (PREssure STaggering Option) scheme, although computationally more expensive, was used to interpolate the pressure term as it directly calculates the pressures at cell faces and avoids interpolation errors. The interface was determined by the Geo-Reconstruct Algorithm (Youngs, 1982) that uses a piecewise-linear approach to determine the interface between fluids. Firstly, the algorithm assumes that the interface between two fluids has a linear slope within each cell based on volume fractions. It then uses this linear shape for computation of the momentum transport by advection of fluid through the cell faces. Finally, it calculates the volume fraction in each cell using the balance of fluxes computed from the previous step. To account for the interfacial forces, the Continuum Surface Force (CSF) model (Brackbill et. al., 1992) has been formulated such that the addition of surface tension to the VOF calculation results in a source term in the momentum equation. It creates the interface between the two liquids as a transition region of finite thickness where the surface tension force term is proportional to the curvature in each location. Outside the interface, this force term is zero. A first order implicit scheme was used for time discretization with a maximum Courant number of 0.25. For all residual values, the convergence tolerance achieved within each time-step when monitored, was found to be $<10^{-6}$. The computations were carried out at Sheffield Hallam University's High-Performance computing cluster.

### *2.5. Test for Mesh Independency*

To evaluate the mesh independency, simulations were performed by constructing five meshes with the resolutions $\Delta r = \Delta z = 0.02\ mm$, $\Delta r = \Delta z = 0.025\ mm$, $\Delta r = \Delta z = 0.04\ mm$, $\Delta r = \Delta z = 0.07\ mm$ and $\Delta r = \Delta z = 0.1\ mm$ that were uniform throughout the computational domain mentioned previously. Fig.2 shows the time evolution and pinch-off of the drop

measured as a function of growing length $\frac{L}{D_0}$ for various mesh sizes where *D=0.584 mm,* $Bo = 0.045$ and $Re = 233$ ($We = 1.28$). Whilst the growing length and breakup times show differences for mesh sizes 0.07 *mm* and 0.1 *mm* with respect to the finest mesh case examined namely the $\Delta r = \Delta z = 0.02\ mm$, the agreement gets better with a mesh size of 0.04 *mm* and almost identical results are observed with 0.025 *mm* mesh size.

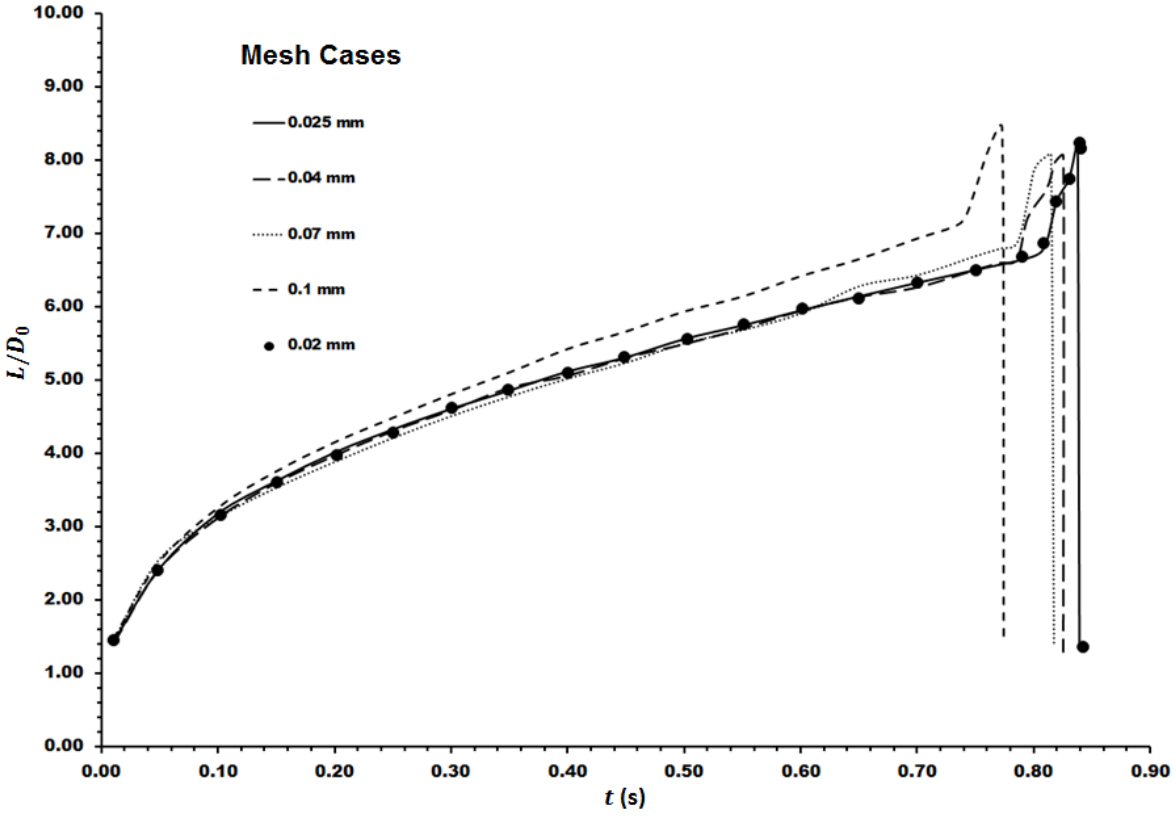


**Fig.2.** Time evolution of a droplet for various mesh cases for off for *We*=1.28, *Bo*=0.04596 and *D*=0.584 mm ($D_0$=0.902 mm).

Fig.3a shows the volume fraction distribution of the droplet just prior to pinch-off. Numerical diffusion is observed at the interface as well as within the drop for coarse mesh cases whereas with higher refinement levels, good agreement is evidenced from both spatial as well as from a temporal perspective for mesh cases 0.02 and 0.025 *mm* respectively. Fig.3b shows the total pressure of the drop on the iso-surface of the liquid volume fraction distribution where maximum total pressure experienced by the drop is seen at the necking region.

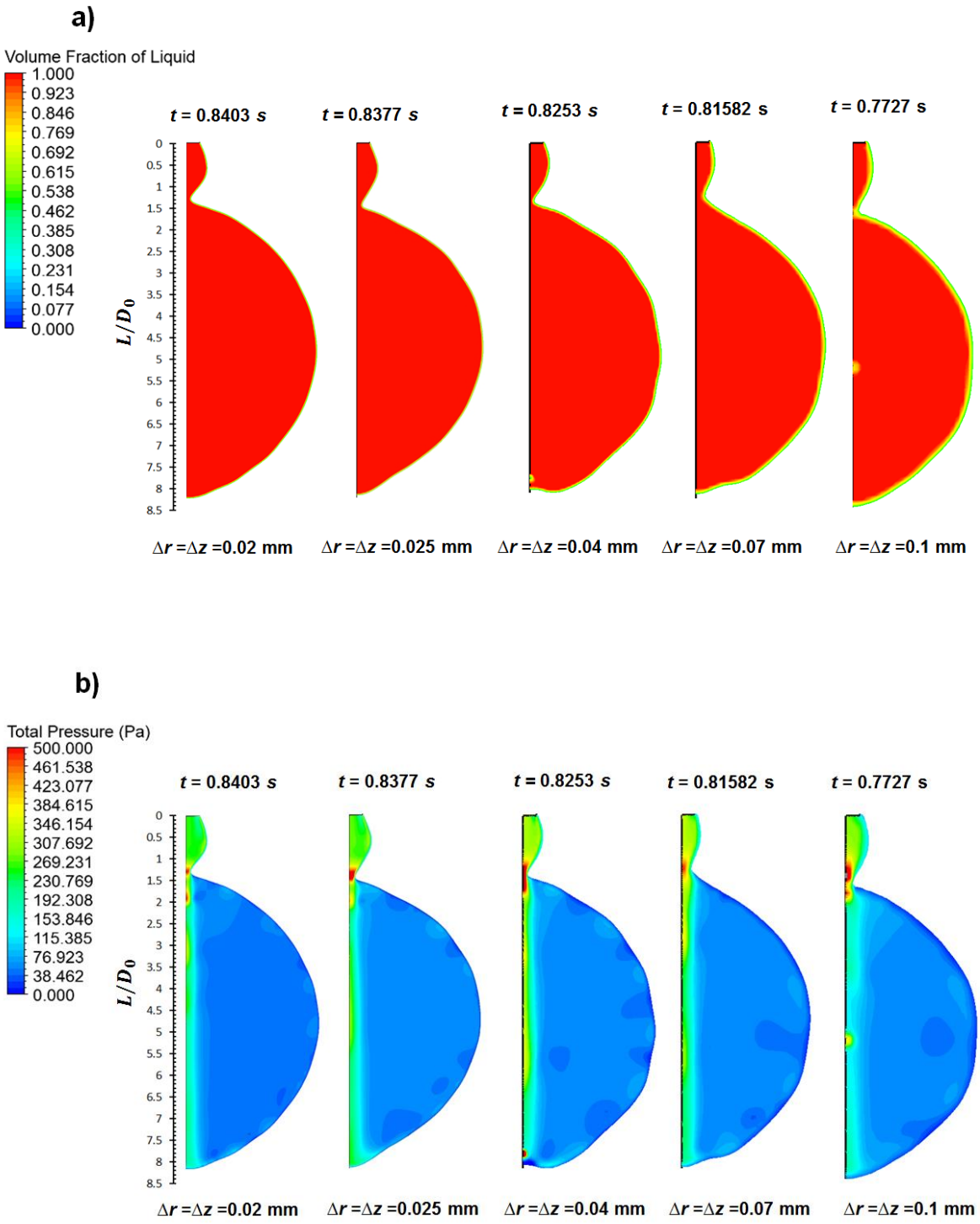


**Fig.3.** a) Volume fraction and b) Total pressure distributions for a droplet shown during necking for various mesh cases for *We*= 1.28, *Bo*=0.04596 and *D*=0.584 mm ($D_0$= 0.902 mm).

With mesh cases 0.02 *mm* and 0.025 *mm*, the agreement is observed to be much closer and differences in the total pressure distribution are seen to be almost insignificant in describing the formation and pinch-off of droplets. Considering the computational cost and the large number of simulations required for this study, it was very time-consuming to employ the finest mesh case for all the simulations. However, considering that a good overall agreement the mesh size $\Delta r = \Delta z = 0.025\, mm$ has with the finest mesh case presented, a mesh size of 0.025 *mm* was used for the whole computational domain.

## 3 Results and Discussions

In this section, we present dynamics of droplet formation and breakup in periodic, dripping faucet and the jetting regimes. Increasing the flow rate leads to transition from dripping to jetting regimes and such a transition can be characterized using first and second limits. The first limit defines the threshold velocity for which transition occurs from periodic to quasi-periodic emission of droplets. The second limit however, defines the velocity for which the drop disintegration moves downstream to distances where $L/D$ > ~10. Fig.4 presents the validation of our simulations for various orifice diameters shown in Table.2. with the experimentally determined limits of transition that were reported earlier by Clanet and Lasheras (1999).

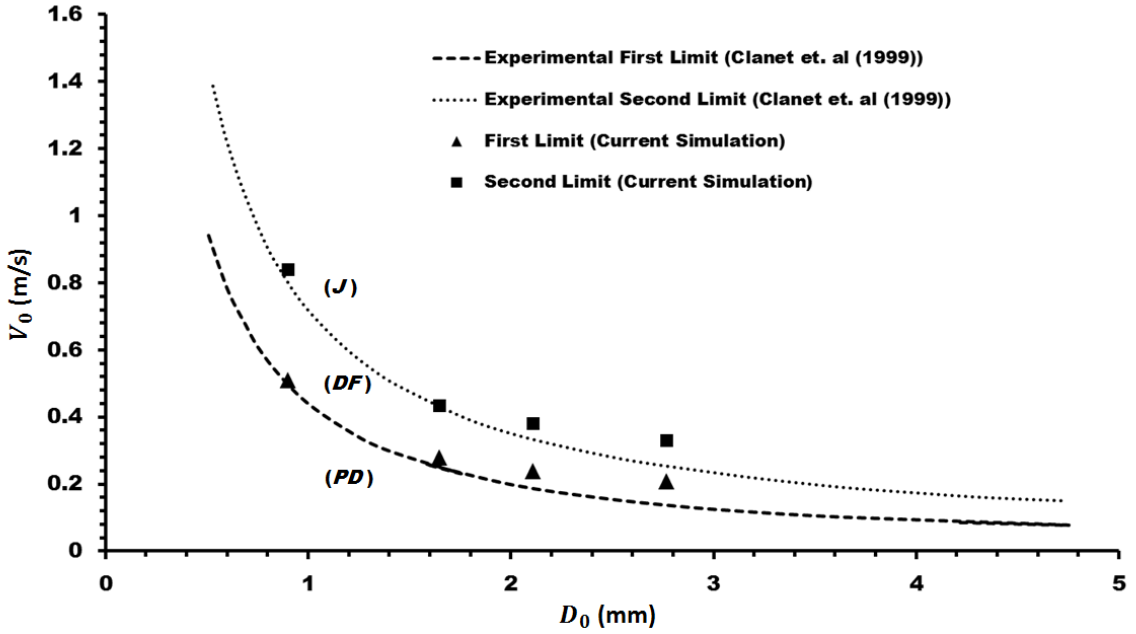


**Fig.4.** Comparison between the current numerical simulations and experimental results from Clanet and Lasheras (1999) for periodic dripping (*PD*) characterized within the first limit, dripping faucet (*DF*) within the second limit and the jetting regime beyond the second limit.

As seen in Fig.4, with increase in orifice diameters, the first and second limit regimes start to narrow. It is seen that the discrepancy between numerical and experimental data for both the first as well as the second limit is greater where the boundaries of the limits are closer and pertaining to (*DF*) regime getting significantly narrower. Although differences are observed quantitatively for larger orifice diameters, qualitatively however, a good match is seen between numerical and experimental results in distinguishing the first and the second limits at smaller diameters and predicting the trend observed in the experimental results by Clanet and Lasheras (1999). In the following sections, we will focus on our numerical findings of droplet formation and disintegration in each of the (*PD)*, (*DF)* and (*J)* modes and compare them with previously published experimental data, where available.

### *3.1. Periodic Dripping*

Within the regime of the first limit where periodic dripping (*PD*) mode exists, at very small flow rates, there exists a regime where, alongside the primary droplets, satellite droplets are

observed (Zhang and Basaran; 1995; Zhang and Stone 1997; Wilkes et. al., 1999; Zhang, 1999; Notz et. al., 2001; Yildirim et. al., 2005; Subramani et. al, 2006). However, by increasing *Q* beyond a threshold, drops pinch-off at regular intervals and have the same detachment position. This is identified to be the period-1 response to droplet disintegration. Fig.5 shows the time (*t*) evolution of four consecutive drops predicted by the present numerical simulations that have nearly identical growing length $\frac{L}{D_0}$ and with the detachment point ~1$D_0$. The current numerical prediction on the growing length and detachment point for the (*PD*) regime is found to be consistent with the experimentally reported results from Clanet and Lasheras (1999) for the parameters used in this study.

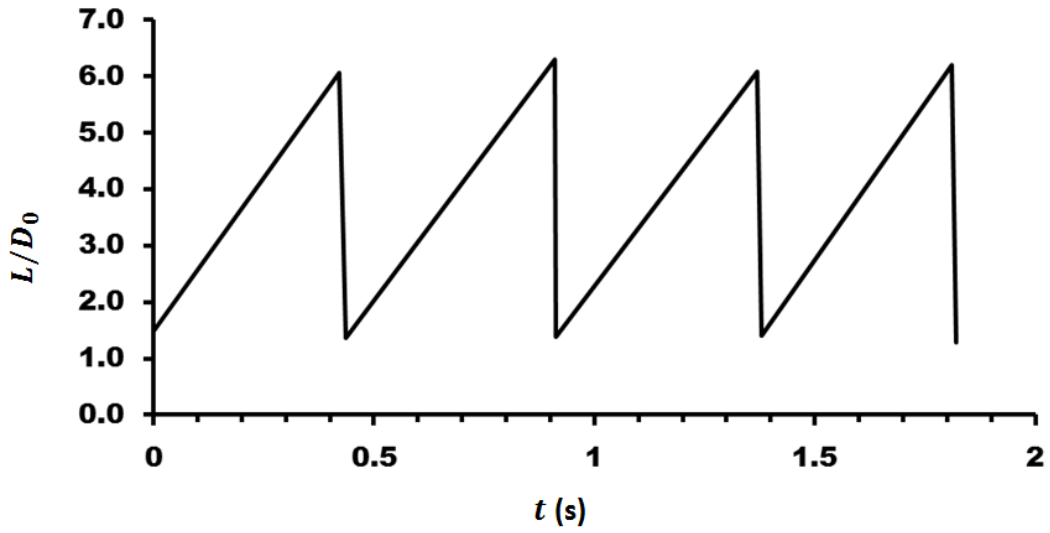


**Fig.5.** Temporal evolution of a droplet formation and growth rate histories for *We*=0.354, *Bo*=0.345 and *D*=1.6 mm ($D_0$= 2.108 mm) in the periodic dripping regime.

Experimentally, it was observed by Clanet and Lasheras (1999) that the time evolution of the necking diameter $D_{neck}$, takes an exponential functional form $D_0\left(1-e^{\frac{(t-t_0)}{t_n}}\right)$ where $t_n$ represents the necking time and $t_0$ is the time shift due to exponential decay where one is expected to observe the onset of instability. Fig.6 shows a comparison of the current numerical prediction of time evolution of neck with experimentally reported results by Clanet and Lasheras (1999). Although we see a difference in the evolution of neck in numerical results; which tends to be faster at compared to the experimental data, it can be observed that the onset of necking and the overall pinch-off period predicted by numerical results shows a good match with the experimental data. One may note that in the experiments the droplet is pinned to thickness of the tube unlike that in the simulations where the thickness is neglected. The results from Fig.6 is analogous to the trend noted by Clanet and Lasheras (1999) who showed that the neck evolution is faster for smaller diameters. The trend shown in Fig.6 suggests that the outer diameter could be influential during neck evolution although drop length and capillary breakup time remain unaffected. In the Fig.7, we show the volume fraction and total pressure distribution profiles during the evolution of the neck and pinch-off for the drop corresponding to Fig.6 for consistency. At the instance of pinch-off ($t$-$t_0$ =-0.0015(s)) shown in Fig.7a), the interface overturning (Day et. al., 1998; Casterjón-Pita et al.,2011; Borthakur et. al., 2017) which is expected for low viscosity fluid, such as water, is clearly predicted by the present numerical result. During the evolution of the neck, the numerical results show that the pressure energy (Fig.7b) spreads along the axis of the drop before pinch off and the maximum total pressure is closest to the neck during breakup.

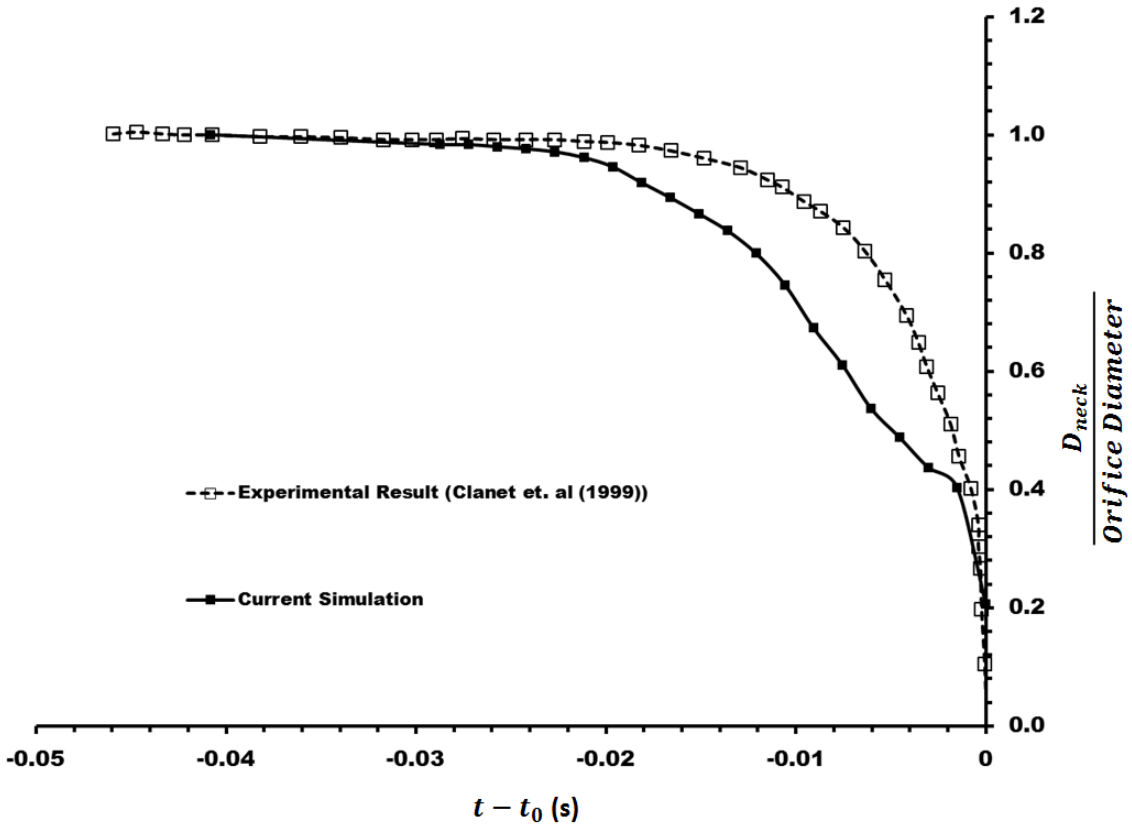


**Fig.6.** Time evolution of the neck for current numerical simulations compared with experimental results from Clanet and Lasheras (1999) for *We*=1.28, *Bo*=0.04596 and *D*=0.584 mm ($D_0$= 0.902 mm)

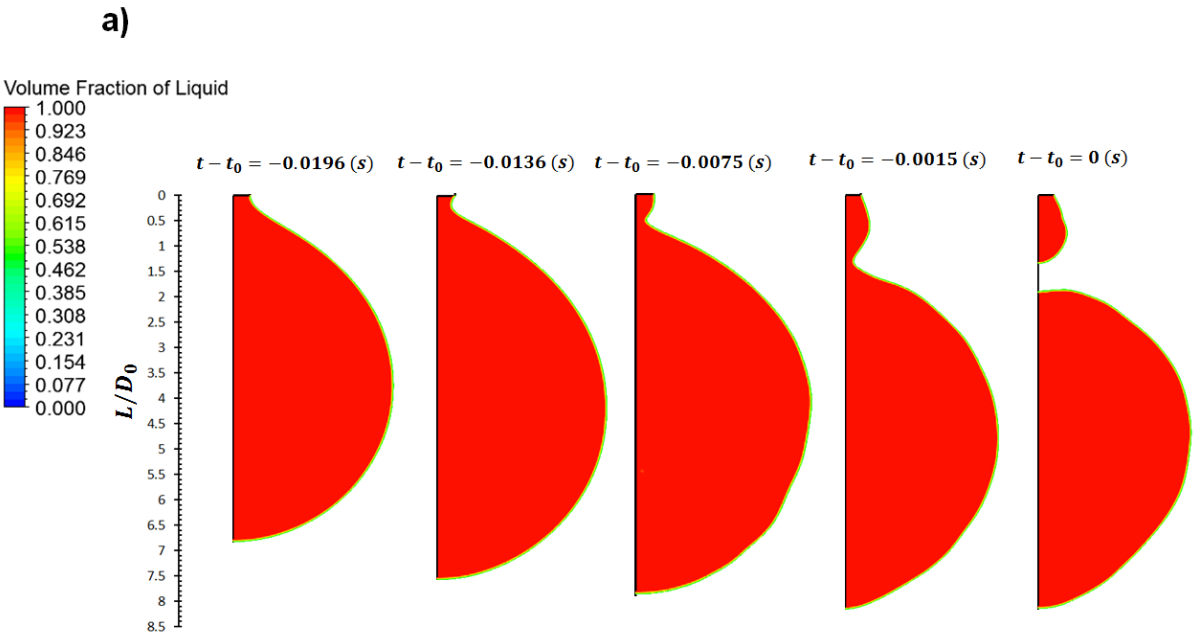

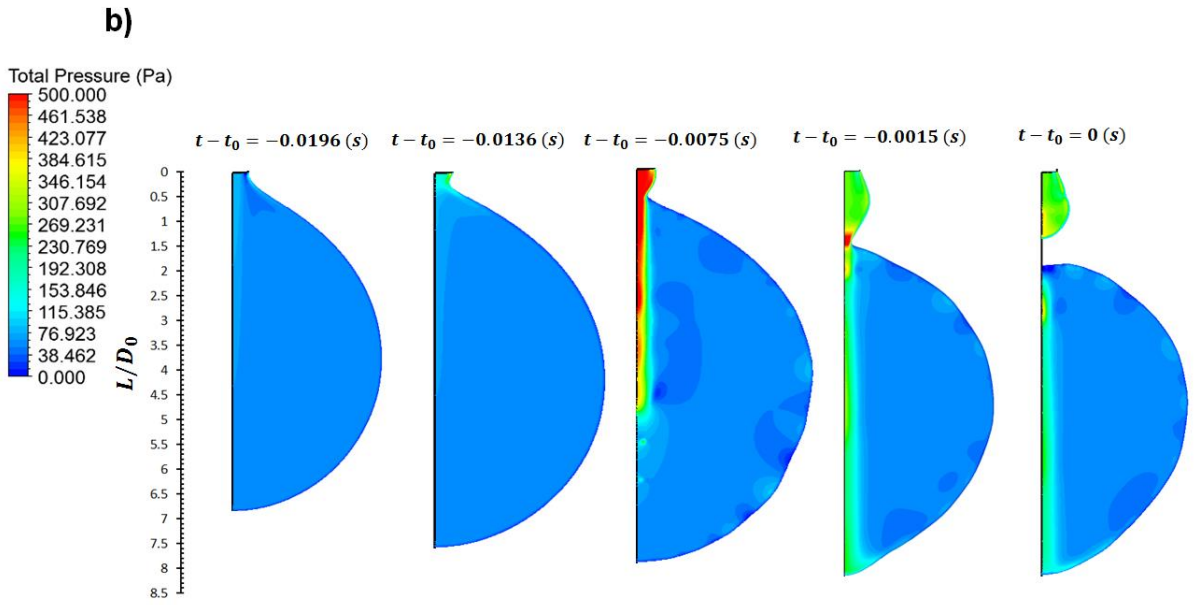


**Fig.7.** a) Volume fraction and b) Total pressure distributions for a droplet showing spatial and temporal evolution of necking and pinch-off for *We*=1.28, *Bo*=0.04596 with *D*= 0.584 mm ($D_0$= 0.902 mm).

### *3.2. Dripping Faucet: Modes of Satellite Drop Formation and Merging*

On reaching the first limit, one enters the (*DF*) second regime where drop emissions are no longer a constant both spatially as well as temporally. Experiments and numerical simulations in the past have shown that high viscosity fluids such as a syrup, with the increase in *Q*, it is possible to transition directly from period- 1 dripping to jetting without exhibiting the intermediary (*DF*) regime (Ambravaneswaran et. al, 2004). However, in the case of low viscosity liquids such as for water, the (*DF*) regime could exhibit a range of complex dynamics (Sartorelli et al., 1994) starting from period- 2, period- 3, period- 4 etc., and then to chaotic responses before transitioning to a jet (Clanet and Lasheras, 1999; Coullet et. al., 2005; Subramani et al., 2006) when *Q* exceeds a threshold. Fig.8 shows a comparison of drop growth histories between present numerical results with experimental results from Clanet and Lasheras (1999) for a period- 2 response when *We*=1.6 and *Bo*=0.345. The present numerical results show a trend that is evidenced in the experimental data in predicting the existence of two frequencies that correspond to alternate emissions of smaller and larger drops. In addition, the growing and pinch-off lengths for drops for both emission periods predicted by the computational results, for smaller and larger sized drops, show a good agreement with experimental observation. However, we see discrepancies with the drop numbers generated with time between the numerical result and experimental data. Such discrepancies could potentially be attributed to the fact that in the experiments the thickness of the wall of the nozzle considered in the experiments has not been included in the model due to additional complexities involved in accurately describing wall-wetting and fluid-solid interface characteristics. However, to the best of author's knowledge, a comparison of drop histories between numerical and experimental results in the (*DF*) regime corresponding to a period- 2 mode, for water is reported for the first time.
Fig. 9 shows the volume fraction profiles of the smaller and larger drop distributions that evolve in the period- 2 regime for the same parameters as in Fig.8.

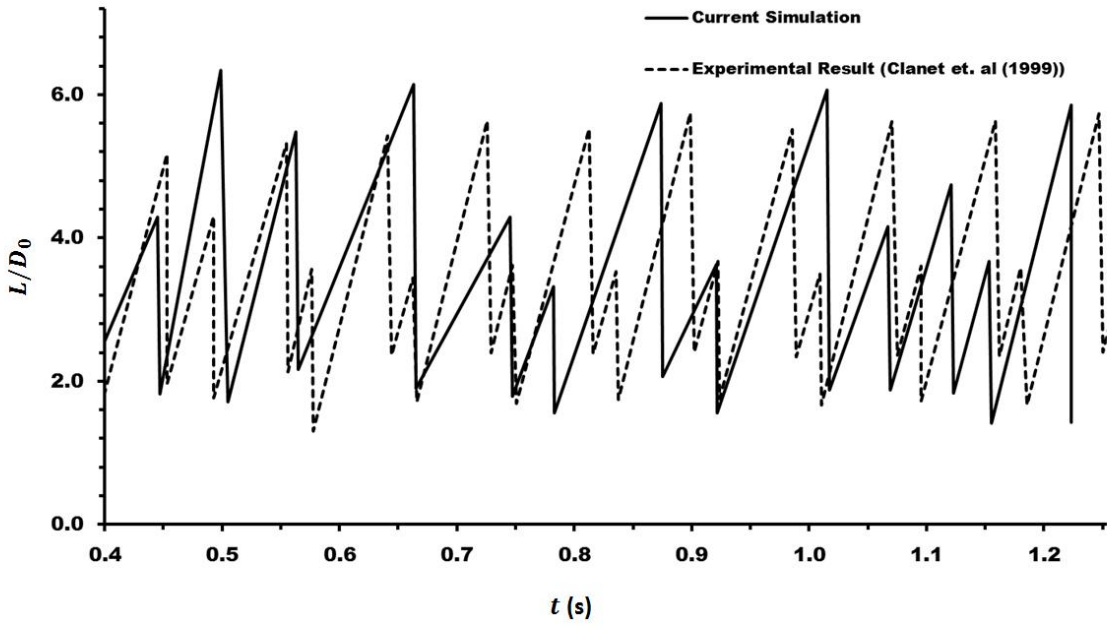


**Fig.8.** Comparison of temporal evolution of the dripping faucet regime from the present numerical simulations showing a period-2 response trend against the experimentally determined growth rate histories from Clanet and Lasheras (1999) for *We*=1.6, *Bo*=0.345 with *D*=1.6mm ($D_0$=2.108 mm).

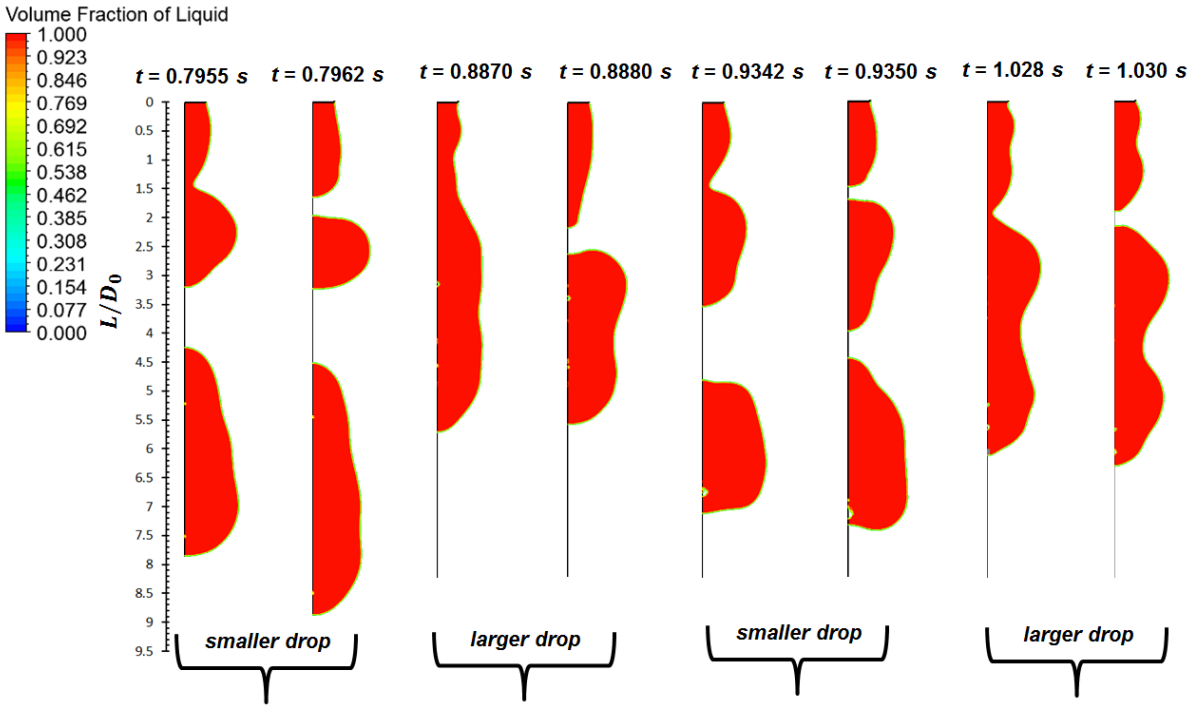


**Fig.9.** Numerical results of the drop distributions and temporal evolution of the dripping faucet regime exhibiting a period-2 trend for *We*=1.6, *Bo*= 0.345 and *D*=1.6mm ($D_0$=2.108 mm).

Interestingly, when the flow rate is increased to a value closer to the boundary of the second threshold limit, it leads to chaotic dripping (*CD*). Fig.10 shows the drop growth histories for *We*= 2.85 and *Bo*=0.345 in the (*CD*) regime, where a combination features corresponding to responses such as a period-2, period-3 etc., seem to exist. Although one could also notice an appreciable increase in drop emission frequencies, we are unable to conspicuously classify such changes as chaotic to non-chaotic transitions leading to a *boundary crisis* as observed by Sartorelli et al., (1994). Potentially, this may be due to the overall computational time that the simulations have been carried out to categorically ascertain such transitions.

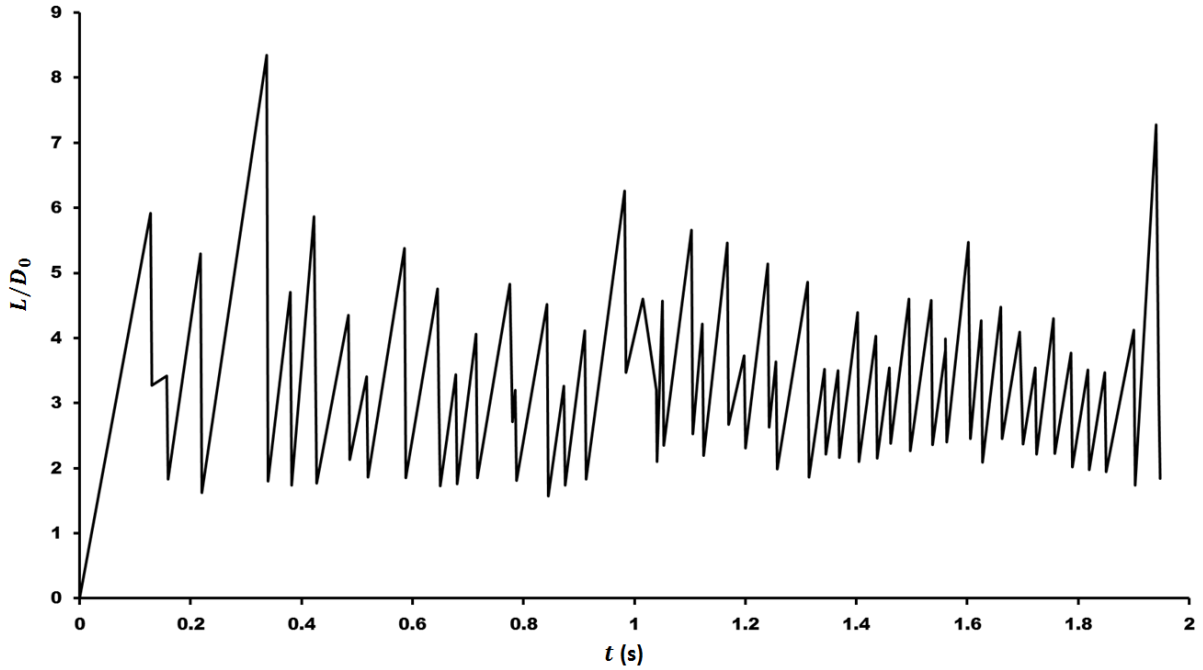


**Fig.10.** Temporal evolution of the dripping faucet regime in chaotic dripping (*CD*) mode showing growth rate histories for *We*= 2.85, *Bo* = 0.345 with *D*=1.6mm ($D_0$= 2.108 mm).

More recently, at relatively high Bond numbers, numerical simulations from Chakraborty et. al., (2016) have identified the existence of satellites in high viscosity liquids in the period-2 regime, namely the period-2s, which has been also been reported in the experimental results from Rubio et. al., (2018). In the current paper we examine the formation of satellite drops in the (*CD*) regime and their merging modes for a low viscosity fluid namely, water. We focus only on the mainstream liquid and first primary drop that disintegrates from the mainstream liquid and any satellite drop(s) that are formed or associated within them. Specifically by focusing our attention on the motion of primary and satellite drop shown in Fig.11, one may observe that they tend to show oscillatory pattern when moving downstream by exhibiting characteristics of alternative *stretching* and *shrinking* in stream-wise and span-wise directions and vice-versa. Such oscillations in droplets are strongly nonlinear and their decay has been attributed to viscous damping (Becker et. al., 1991). Broadly, such oscillations in droplets are generated due to mechanisms such as breakup from mainstream, through coalescence or due to bouncing (Suñol and Cinca, 2015). Within this focus, our current numerical simulations predict plethora of interesting dynamics that identify four possible modes of satellite drop formation and coalescence as described in Fig.11. In Fig.11a), we observe that a liquid thread like structure that is attached to the mainstream liquid disintegrates forming a satellite drop which merges with the immediate primary drop present downstream. This type of satellite formation and merging has features similar to that of period- 1s which is well known and has been significantly reported by various researchers (Notz. et al., 2001; Chen et. al., 2002).

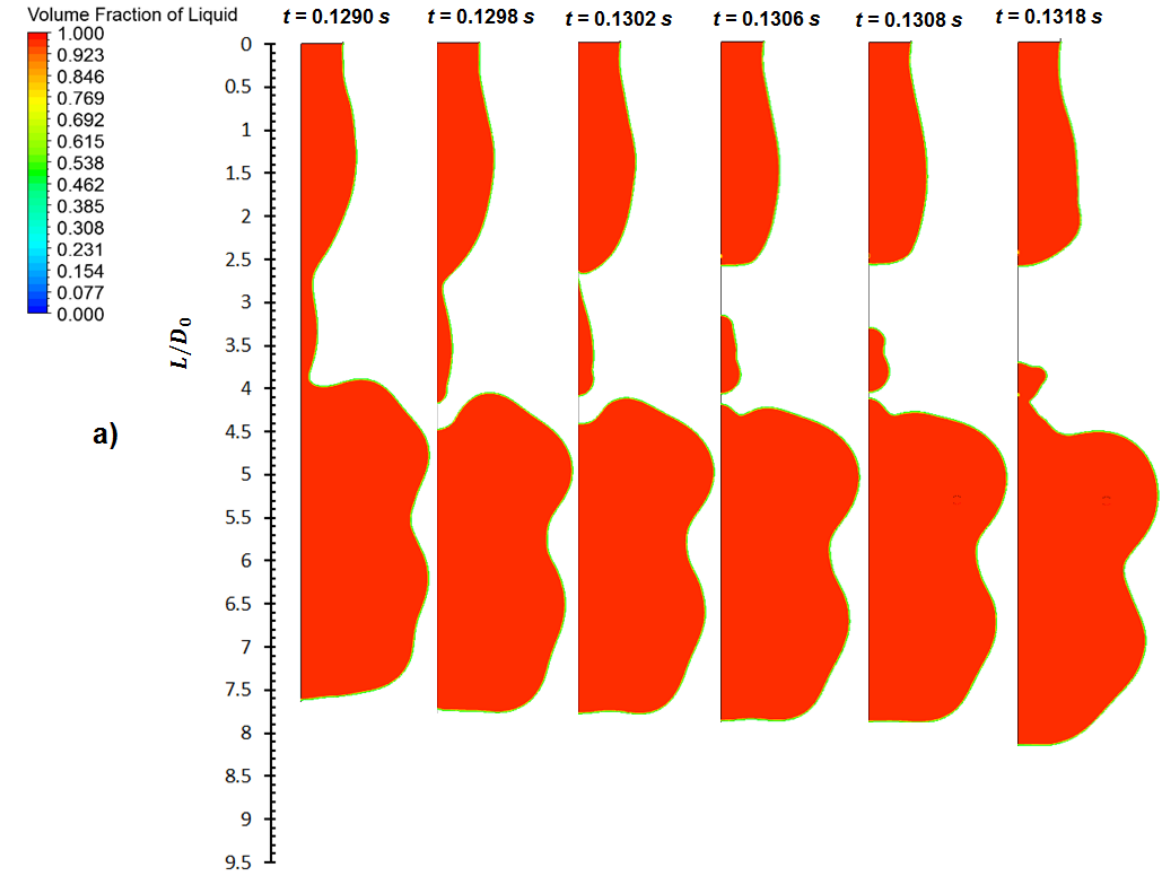
Volume Fraction of Liquid
1.000
0.923
0.846
0.769
0.692
0.615
0.538
0.462
0.385
0.308
0.231
0.154
0.077
0.000
t = 0.1290 s
t = 0.1298 s
t = 0.1302 s
t = 0.1306 s
t = 0.1308 s
t = 0.1318 s
L/D0
0
0.5
1
1.5
2
2.5
3
3.5
4
4.5
5
5.5
6
6.5
7
7.5
8
8.5
9
9.5

a)

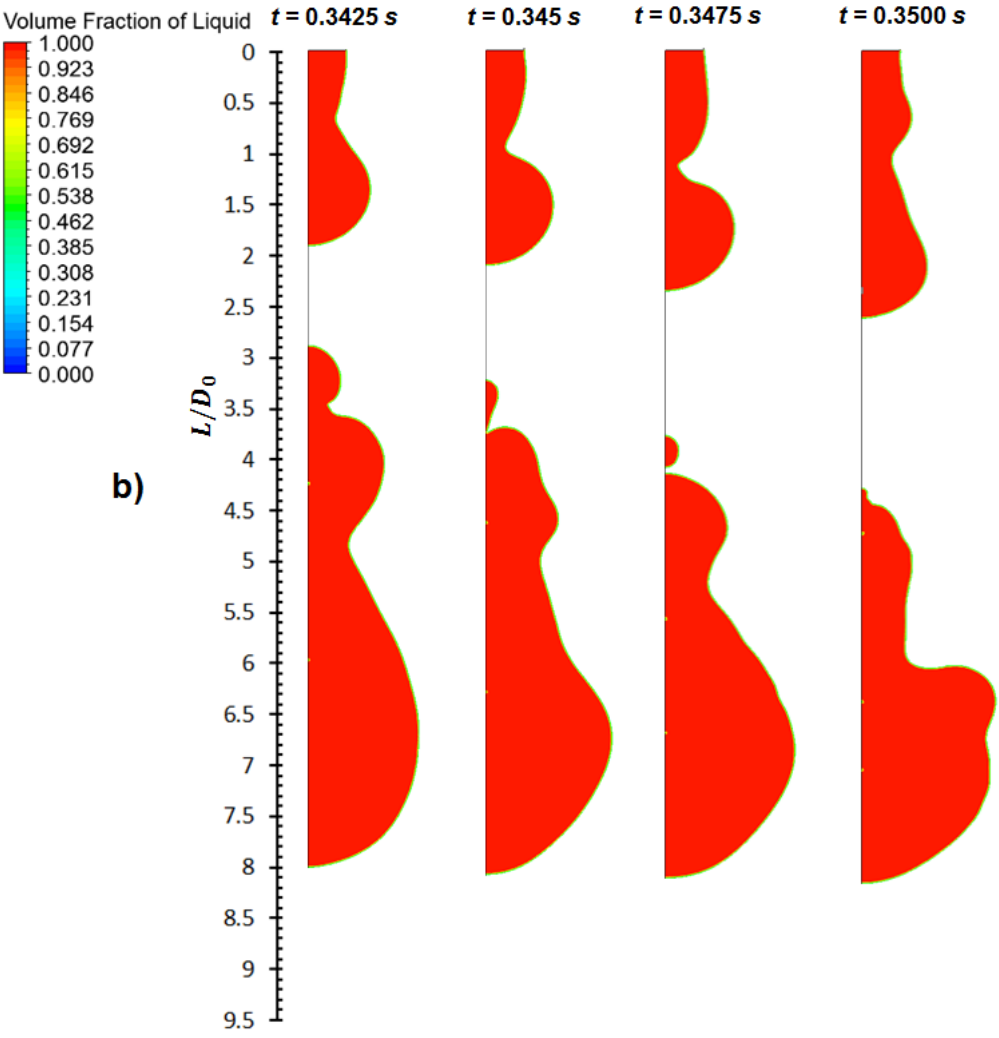
Volume Fraction of Liquid
1.000
0.923
0.846
0.769
0.692
0.615
0.538
0.462
0.385
0.308
0.231
0.154
0.077
0.000
t = 0.3425 s
t = 0.345 s
t = 0.3475 s
t = 0.3500 s
L/D0
0
0.5
1
1.5
2
2.5
3
3.5
4
4.5
5
5.5
6
6.5
7
7.5
8
8.5
9
9.5

b)

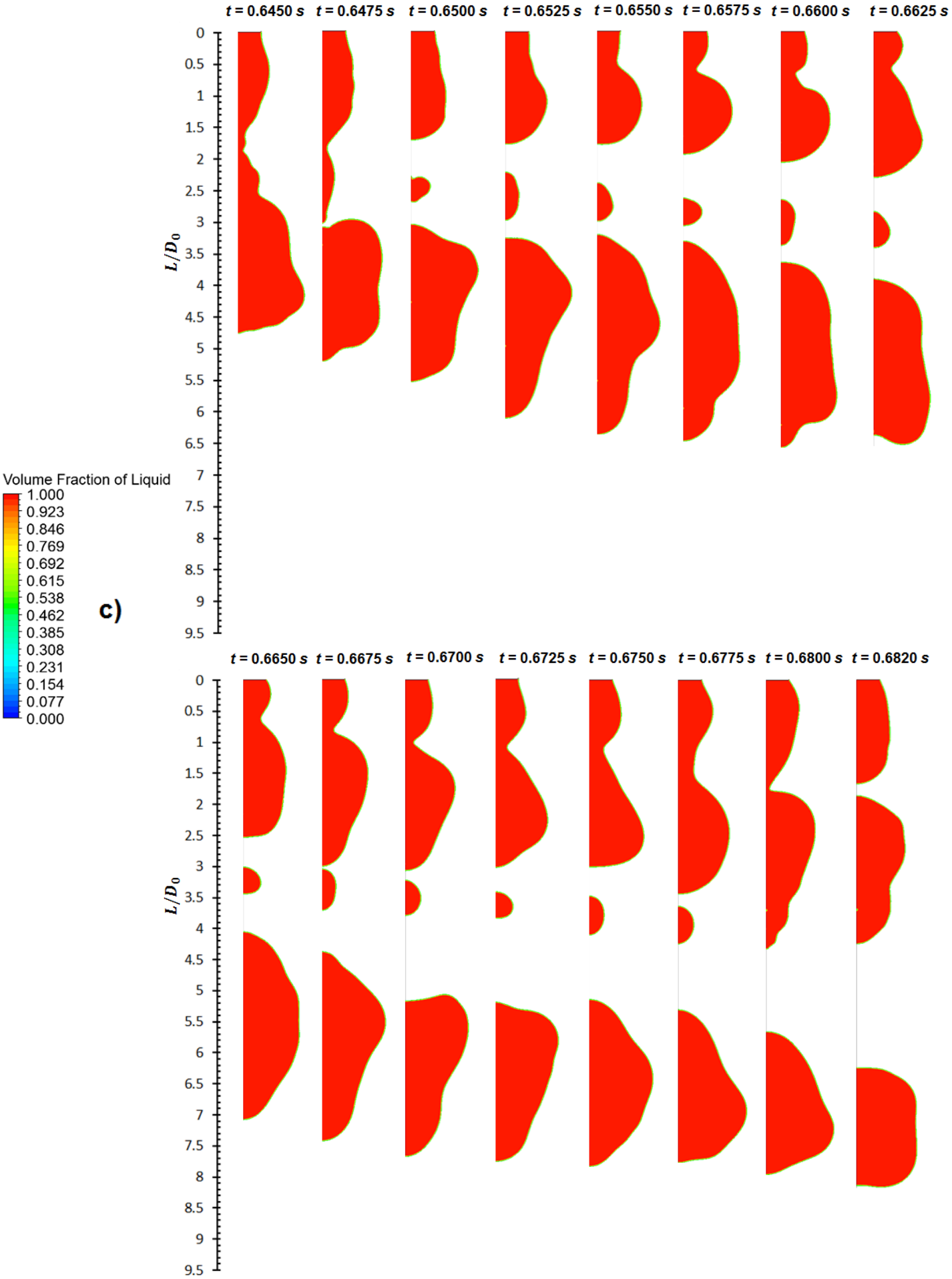
t = 0.6450 s
t = 0.6475 s
t = 0.6500 s
t = 0.6525 s
t = 0.6550 s
t = 0.6575 s
t = 0.6600 s
t = 0.6625 s
t = 0.6650 s
t = 0.6675 s
t = 0.6700 s
t = 0.6725 s
t = 0.6750 s
t = 0.6775 s
t = 0.6800 s
t = 0.6820 s
L/D0
0
0.5
1
1.5
2
2.5
3
3.5
4
4.5
5
5.5
6
6.5
7
7.5
8
8.5
9
9.5
Volume Fraction of Liquid
1.000
0.923
0.846
0.769
0.692
0.615
0.538
0.462
0.385
0.308
0.231
0.154
0.077
0.000

c)

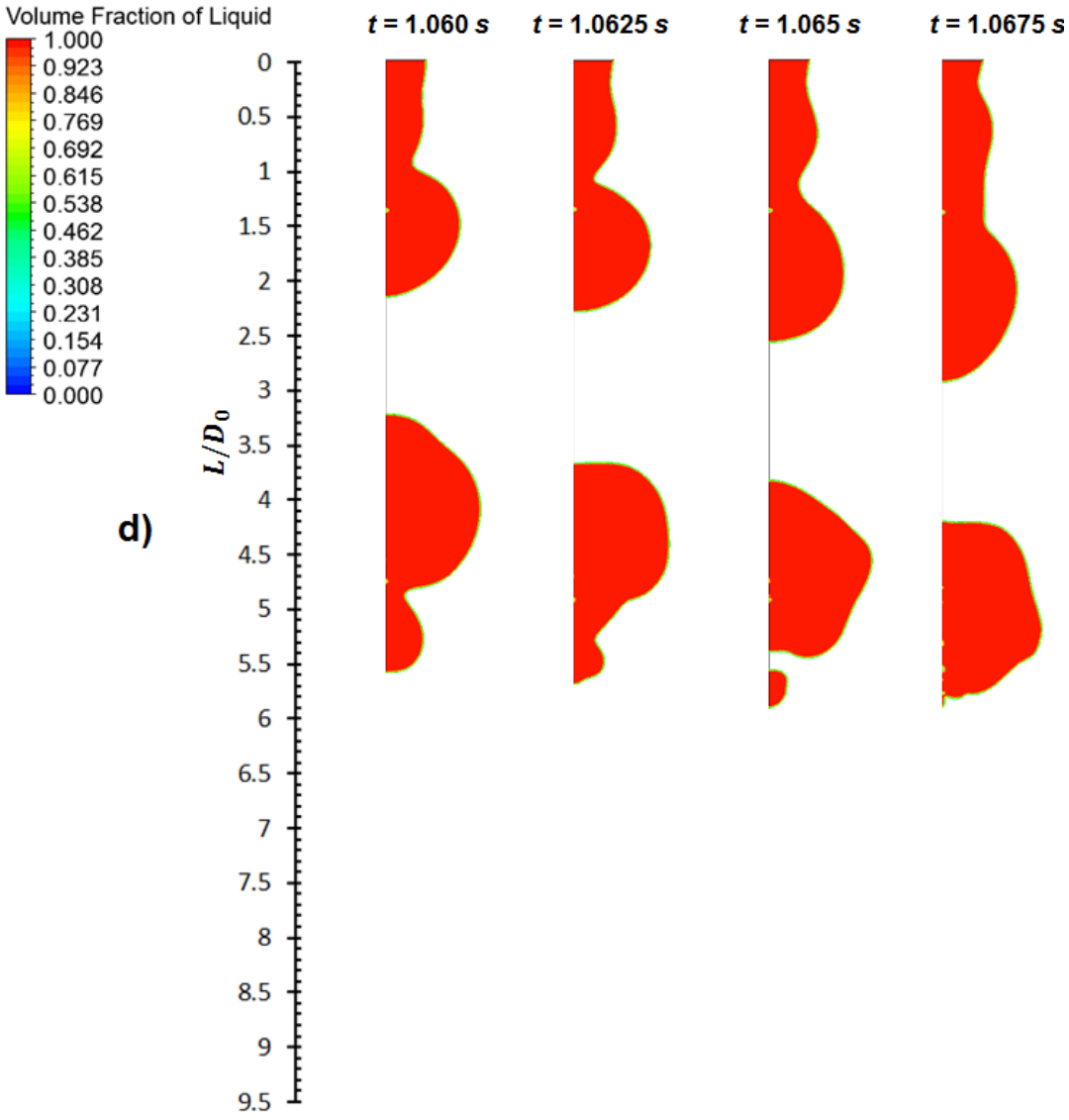


**Fig.11.** Formation of satellite droplets from a) mainstream and merge into primary droplet, b) anterior of the primary drop and merge into primary droplet c) mainstream and merge into mainstream and d) posterior of the primary droplet and merge into primary droplet for *We*=2.85, *Bo*=0.345 with *D*=1.6mm ($D_0$=2.108 mm).

Fig.11b) shows another type of formation of satellite droplet from a primary droplet that was formed from the mainstream liquid. In this case, we observe that the oscillations of the primary drop are non-uniform when moving downstream and depending on its initial shape can aid to the formation of a satellite drop. One such formation is shown in Fig.11b) where the satellite drop is formed from the anterior of the primary drop that moves down with oscillations as described above. Once the satellite drop is formed, almost immediately, we see that it merges with the primary drop. This is owing to the fact that the satellite drop also undergoes oscillatory motion alongside the primary drop when moving downstream, they merge to an equilibrium shape until no further breakup is experienced and due to subsequent decay of oscillations due to viscous damping. Fig.11c) shows the formation of satellite drop from mainstream liquid thread with formation features similar to Fig.11a). But in Fig.11c) we observe that unlike the coalescence of the satellite drop with the primary droplet present downstream shown in Fig.11a)), the mainstream liquid that moves downstream merges with the satellite drop. Another mode of formation of satellite droplet is predicted which is in contrast to Fig.11b), where the satellite droplet is formed from the posterior of the

primary drop as shown in Fig.11d). Although not all primary drops or their instances of pinch-off lead to formation of liquid threads in mainstream that create satellites, we observe that the satellites are formed depending on the initial droplet distribution of the primary drops that are formed from the mainstream liquid and the nature of oscillatory motion associated with them when moving downstream.

### *3.3. Jetting: Varying Jet Breakup length and Coalescence of drops downstream*

After a series of aforementioned transitions and by crossing the second boundary limit as shown in Fig.4, a laminar liquid jet originates where the droplet disintegration point suddenly moves downstream to distances where *L/D* greater than 10. This marks the beginning of the jetting regime with interface perturbations leading to a varicose deformation of the jet. In this study we limit our numerical simulations to Rayleigh jetting regimes and other higher order regimes are beyond the scope of this study. The mean breakup length of a jet has been experimentally determined by Sallam et. al., (2002) for low viscosity liquids, given by the following correlation:

$$\frac{L}{D} = 5\,We^{0.5} \quad \text{valid for } We < 400. \tag{12}$$

In testing the numerical accuracy of the jet length, we take an approach which is similar to that presented by Pan and Suga, (2006) where, the mean breakup length of the jet from their numerical simulations were compared against the correlation given in Eq.12. by Sallam et. al., (2002). Fig.12 shows both the instantaneous and time averaged jet length(s) just before the breakup of droplet occurs. To note, the parameters in the Fig.12 correspond to a mean velocity $V_0 = 0.92\ m/s$ (as shown in Fig.4); which indicate a value that lies closer to the second boundary limit and that the laminar jet has just evolved with an average breakup length of *L*/*D*=~10.96. This behavior matches very well with the experimental results and observations by (Clanet and Lasheras, 1999) shown in Fig.4. Also, we see in Fig.12 that the jet breakup length predicted by the numerical result varies with time. Observations on varying jet breakup length have been evidenced in the past both experimentally (Clanet and Lasheras, 1999) and numerically (Pan and Suga, 2006; Delteil et al., 2011; Chakraborty et. al., 2016; Borkathur et. al., 2017) by several researchers.

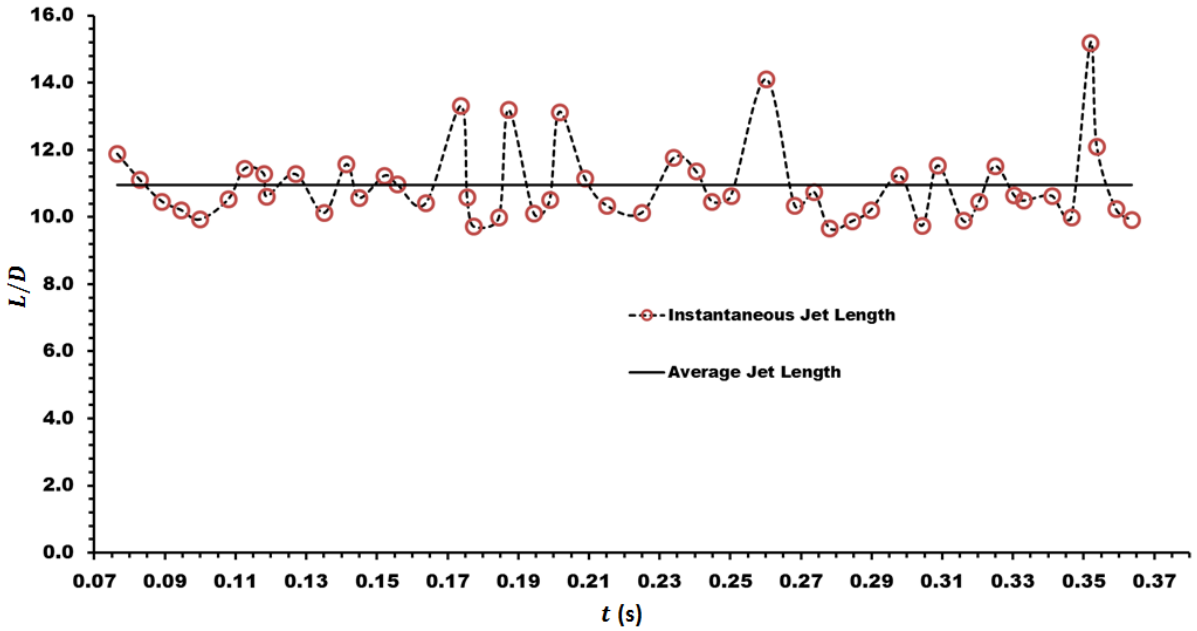


**Fig.12.** Instantaneous and time averaged jet extensions at the inception of breakup for *We*=6.8, *Re* = 537, *B0*=0.0459 with *D*= 0.584 mm ($D_0$= 0.902 mm).

Fig.13 shows the numerical results for varying *We* obtained by monitoring jet lengths for >70 drop disintegrations in each case; typically, a value that is much greater than previously reported numerical results for jet lengths. For each *We* values, we present the instantaneous minimum, maximum and time averaged jet lengths and compare against the experimental correlations by Sallam et. al., (2002) shown in Eq.12 for the same *Bo*=0.0459 by maintaining the orifice diameter. Subsequently, we also compare the numerical results with Eq.12 when *We* is maintained to be a constant for different Bond numbers (by varying the orifice diameter) shown in Table.3 For all the cases presented, we see that the time averaged breakup length shows reasonably good agreement with the experimentally observed correlation from Sallam et.al.,(2002). Incidentally, we note that with the jet breakup varying with time for free laminar jets, the numerical results present evidences of droplets coalescing when they move downstream. We shall elucidate the coalescence behavior of droplets from the images corresponding to the results presented in Table.3.

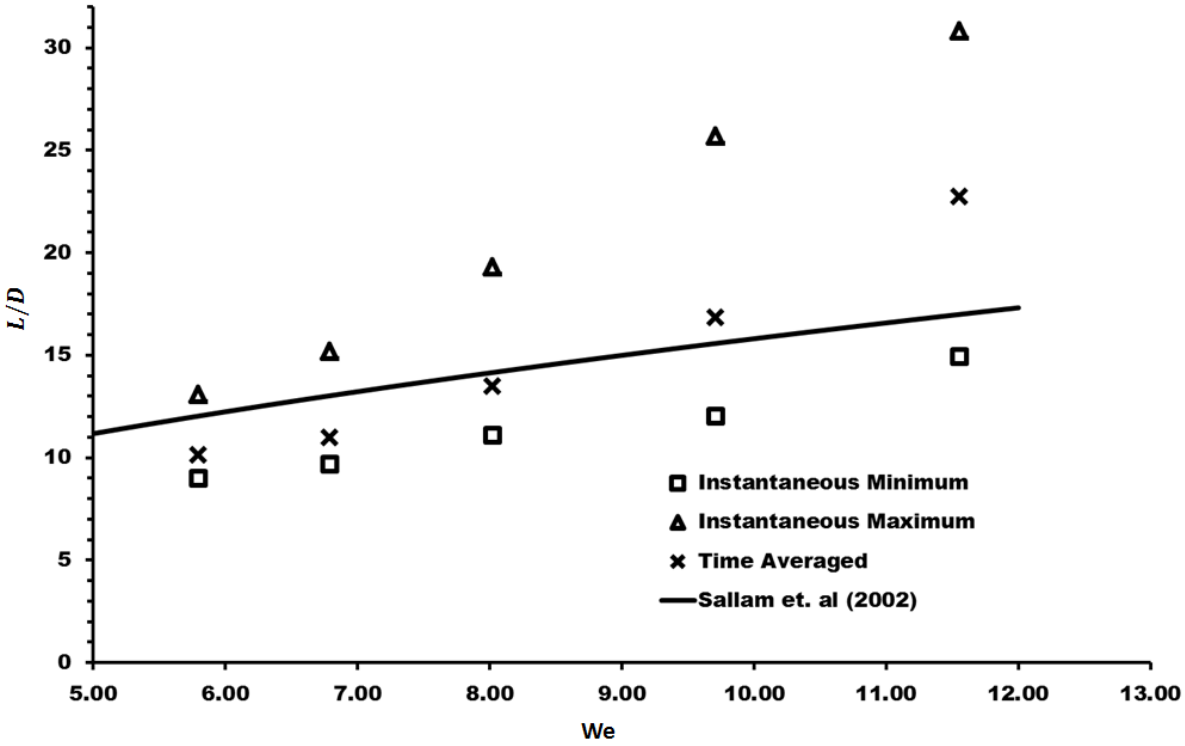


**Fig.13.** Comparison of experimental correlation for jet breakup lengths from Sallam et. al., (2002) given by (Eq. 13) with present simulation for various Weber numbers with *Bo*=0.0459, *D*=0.584 mm ($D_0$=0.902 mm).

| *D (mm)* | *Bo* | *Re* | *We* | *Experimental fit from* Sallam et. al., (2002) $\frac{L}{D} = 5We^{(1/2)}$ for $We < 400$ | *Simulation Results* $\left(\frac{L}{D}\right)$ | | |
|---|---|---|---|---|---|---|---|
| | | | | | *minimum* | *maximum* | *Average* |
| *1.6* | 0.345 | *890* | *6.8* | *13.038* | *9.645* | *16.268* | *12.259* |
| *0.584* | *0.0459* | *537* | *6.8* | *13.038* | *9.664* | *15.184* | *10.96* |

**Table.3.** Values of jet breakup lengths obtained from the present numerical results compared with Sallam et. al., (2002) for two different *Bo* but maintaining the same *We*.

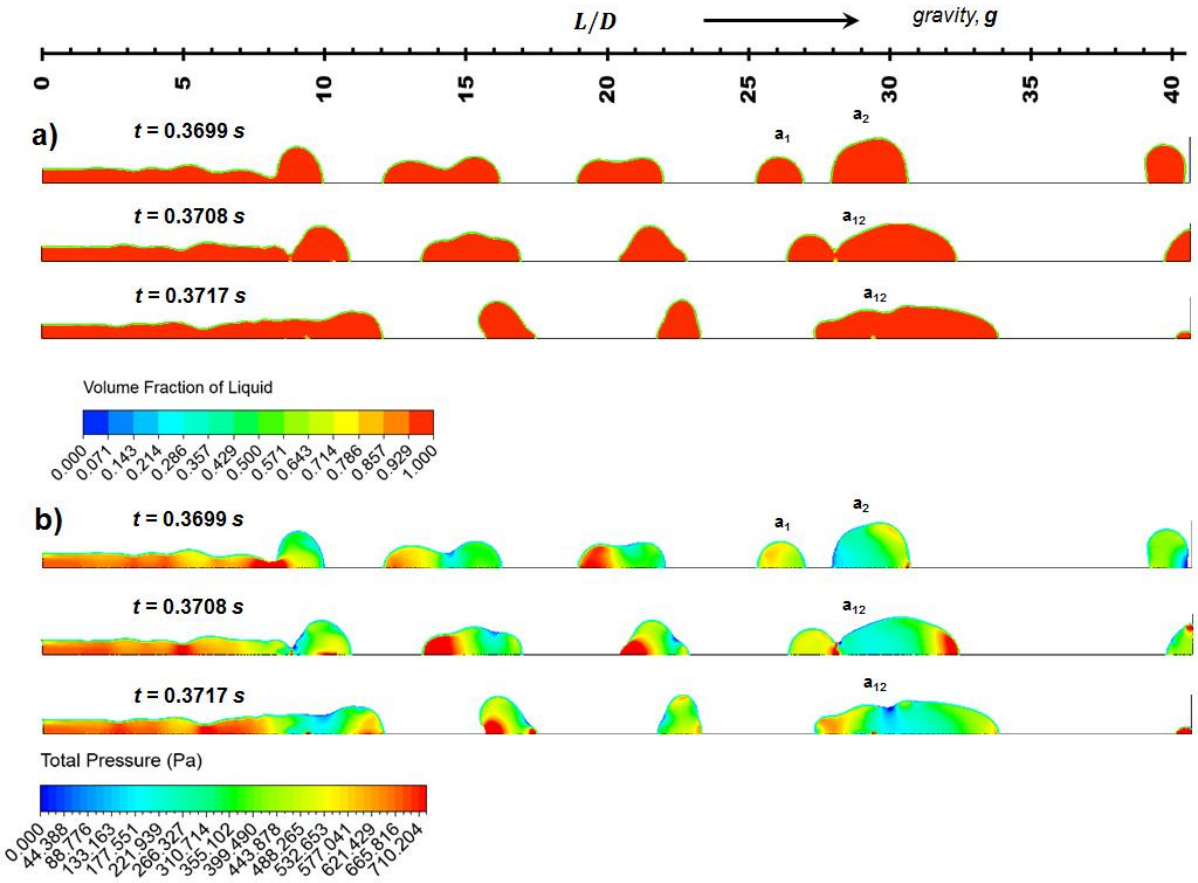


**Fig.14.** Evolution of a Jet and merging of two primary drops downstream shown using a) Volume fraction and b) Total pressure distributions for *We*=6.8, *Re*=537, *Bo*=0.0459 with *D*=0.584 mm ($D_0$= 0.902 mm).

Many critical conditions may lead to drops merging downstream such as, but not restricted to; the variation in breakup length, wavelength of the jet during breakup, drop sizes resulting from diminutive breakup timescales etc., However, in the present study we find that phenomenon of the nature of oscillatory motion of drops as discussed in the Section 3.2, which is a by-product of the aforementioned conditions can aid to the phenomena of merging of droplets downstream.Fig.14 shows the volume fraction and total pressure distributions for a jet with *We*=6.8, *Re*=890, *Bo*=0.3449 where *D*=1.6 mm ($D_0$=2.108 mm) taken at arbitrary snapshots. We see two primary droplets $\mathbf{a}_1$ and $\mathbf{a}_2$ that were formed from the jet ($\mathbf{a}_2$ was formed prior to $\mathbf{a}_1$), moving downstream along with oscillatory motion that is normally mitigated by viscous damping. In the present case, it can be seen that the oscillatory motion experienced by $\mathbf{a}_1$ is synchronous to $\mathbf{a}_2$ with respect to both droplets experiencing a *stretching* motion in stream-wise direction. When drops move closer to each other, such synchronous motion enhances the feasibility of droplets coming into contact and potentially merges and forms a new droplet $\mathbf{a}_{12}$. Also, as seen from Fig.14b), at the incipience of merging, we observe that the total pressure distribution is highest at the region of contact. Similar behavior is observed with Fig.15 where *We* is identical to Fig.14 but for *Re*=890, *Bo*=0.3449 and *D*=1.6 mm ($D_0$=2.108 mm). In all the cases described above, not all primary droplets that are formed coalesce. For both the jets which have the same *We*=6.8 but with different *Bo*, we have shown images of jet evolutions at arbitrary snapshots to reveal coalescence patterns of two primary drops that take place. Interestingly, one may note that in both cases (Fig.14 and Fig.15), the droplets coalesce ~25-29*D*, which typically

corresponds to 2-2.3 times the average breakup length (see Table.3) of the jet observed for cases that are reported with *We*=6.8. We have observed this behavior of coalescence that takes place at various time instances (not shown) for the reported *We* for which, the incipience of coalescence of two primary drops have always taken place only at distances > ~15*D* from the average breakup length of the jet. This suggests that a typical scaling relationship may exist between the average breakup length which is a function of *We* and with the first mean coalescence length within the laminar jet breakup regime.

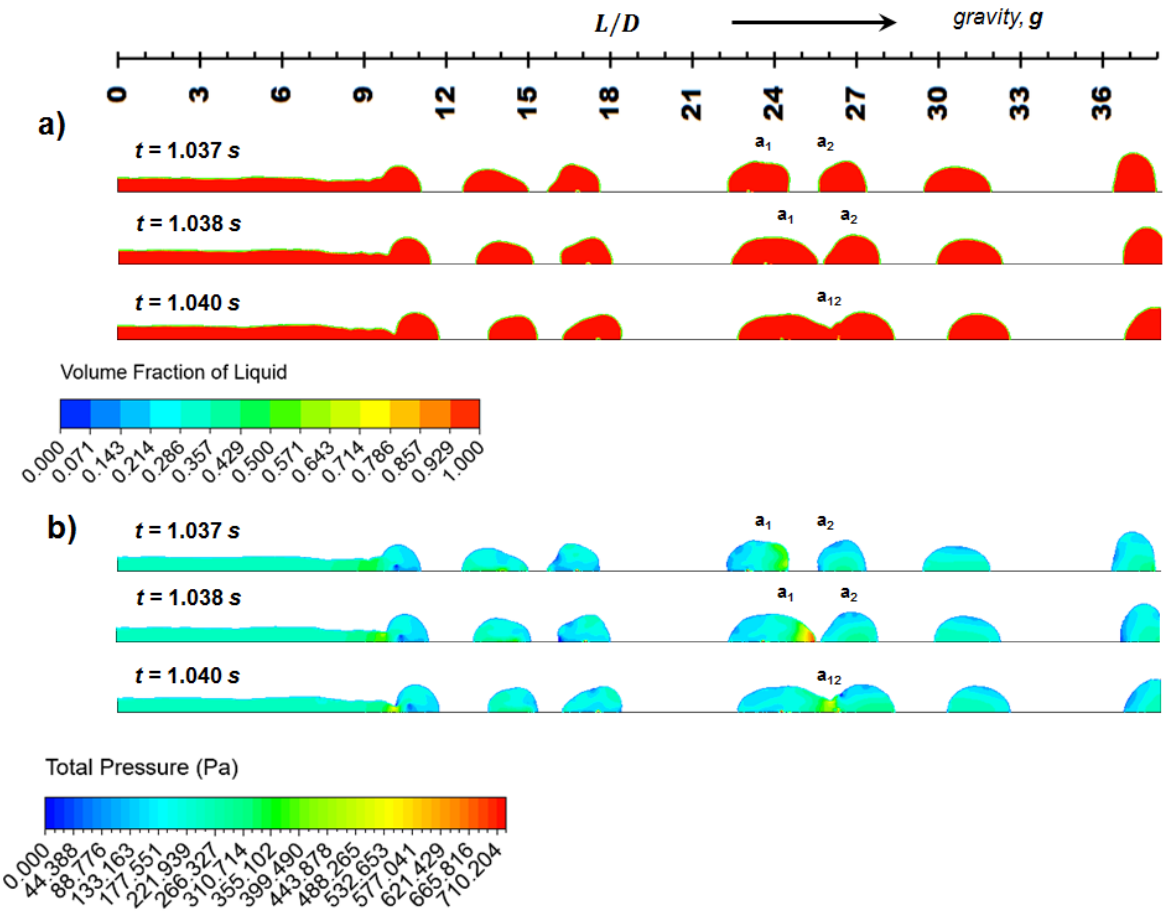


**Fig.15.** Evolution of a Jet and merging of two primary drops downstream shown using a) Volume fraction and b) Total pressure distributions for *We*=6.8, *Re*=890, *Bo*=0.3449 with *D*=1.6 mm ($D_0$= 2.108 mm).

One may note that the jets' transitioned liquid core for both cases show surface features pertaining to low *Re* turbulent behavior. In order to fully characterize such perturbations and to resolve the surface waves in jets due to turbulence, previous studies by Farvardin and Dolatabadi (2013) have pointed out that a full 3D model using Large Eddy Simulations (LES) together with VOF method would be more ideal. We also envisage that the choice of LES-VOF should resolve such higher order surface effects and further enhance the agreement between predicted average jet lengths with experimentally determined results from Sallam et. al., (2002).

## 4. Concluding Remarks

We have presented an axis-symmetric model that comprises the Navier-Stokes equations coupled to Volume of Fluid method and with Continuum Surface Force approach to predict transition from dripping to jetting in a simple Newtonian fluid. ANSYS Fluent (Version 18.0) has been used with Geo-Reconstruct Scheme for interface determination in explicit formulation and with NITA time stepping algorithm. After carefully examining the grid resolution and determining the mesh independency, a series of numerical simulations were carried out for various orifice diameters (*D*) and Weber numbers (*We*) that showed an excellent agreement in predicting the boundaries of the first and second limits corresponding to the regimes of the (*PD*), (*DF*) and (*J*) responses that were experimentally reported by Clanet and Lashreas (1999). At low flow rates corresponding to the (PD) mode within the period-1 response, the numerical results obtained for the droplet necking time predicted a nearly exponential trend and the predicted breakup timescales agree reasonably well with the previously determined experimental results. Whereas, when the flow rate reaches a threshold limit corresponding to the (DF) mode, with the same experimental parameters set in numerical simulations, a period-2 response is predicted agreeing well with experimentally determined drop growth histories and in identifying two emission frequencies. Increasing the flow rate eventually led a route to chaotic dripping (*CD*) response that showed a combination of several periodic responses. The numerical results also featured the oscillatory motion of droplets when moving downstream.

In the (*CD*) response, the numerical results predict four new modes of formation of satellite drops that occur from a thread like structure from the mainstream liquid and either merges with the a) onward moving mainstream liquid or b) with the primary drop next to it downstream. In other cases, the satellites were formed from either the c) anterior or the d) posterior side of the first primary droplet depending on its nonlinear oscillatory motion when moving downstream and its initial shape, that were found to merge with the primary droplet subsequently. By increasing the flowrate beyond the second boundary threshold, the numerical results predict a laminar jet that emanates from the orifice where, typically droplet disintegration occurs at distances $L/D>\sim10$. This result is in excellent agreement with the experimental results from Clanet and Lashreas (1999) for water. Additionally, the results show fluctuations in breakup length of the jet with time similar to the observations reported in earlier studies. The breakup length predicted by the numerical results for different *We* and *Bo* agree reasonably well with the experimentally obtained correlations from Sallam et. al., (2002). We observed that some drops exhibit the tendency of coalescing with the other and provide their merging distances downstream. Typically, we demonstrated with $We=6.8$ and with two different $Bo=0.00459$ and 0.3449, where coalescence of primary droplets take place at distances ~10-12*D* from the breakup location which suggests that a potential scaling relationship may exist with the onset of merging, breakup length and *We*.

Although the above results for the coalescence of drops and the onset of their specific merging distances will need validation from experimental results, we observe from our simulations that depending on the type of the oscillatory motion that is exhibited by some drops moving downstream, the phenomenon of drops coalescing with one another other takes place. Despite well predicting the overall behavior and salient features within the dripping to jetting transitions, one may note that the coalescence of two axis-symmetric primary drops arising from a laminar jet or during modes of dripping may not strictly lead to the formation of an axis-symmetric droplet in which case, the model will exhibit its pitfalls in revealing such formations. Also, recent experiments (Suñol and Cinca, 2015) have demonstrated that in addition to drops coalescing, they also exhibit the characteristics of bouncing when they come into contact one another in certain scenarios; such realizations are beyond the realm of the current set of equations used in the present study. In the future, we aim to extend the current study to describe the onset of coalescence of primary drops and satellites from free laminar jets and present a scaling relationship with dimensionless numbers to quantify their merging length, pattern and timescales.

## Acknowledgements

The author wishes to thank Dr. Tim Spencer for valuable discussions on the subject matter and Mr. Steven Brandon and Mr. Alex Webster for managing the computing resources and HPC support.

This work was supported by ANSYS Academic Research Partnership Grant.

## References

1. Rayleigh, L., 1899. Investigations in capillarity: the size of drops. – The liberation of gas from supersaturated solutions. – Colliding jets. – The tension of contaminated water-surfaces. Phil. Mag. 48, 321–337.

2. Savart, F., 1833. Mémoire sur la constitution des veines liquides lancées par des orifices circulaires en mince paroi. Ann. de Chim. 53, 337–386.

3. Tate, T. 1864. On the magnitude of a drop of liquid formed under different circumstances. Phil. Mag. 27, 176–180.

4. Plateau, J., 1873. Statique expérimentale et théorique des liquides soumis aux seules forces moléculaires (Gauthier-Villars, Trubner et cie, Paris).

5. Rayleigh, L., 1879. On the instability of jets. Proc. Lond. Math. Soc. **10**, 4.

6. Harkins, W.D., & Brown, F.E., 1919. The determination of surface tension (Free surface energy) and the weight of falling drops: the surface tension of water and benzene by the capillary height method. J. Am. Chem. Soc. 41, 499–524.

7. Pitts, E., 1976. The stability of a drop hanging from a tube. J. Inst. Math. AppZ. 17,387-397.

8. Zhang, X., Basaran, O.A., 1995. An experimental study of dynamics of drop formation. Phys. Fluids 7, 1184–1203.

9. Zhang, D.F., Stone, H.A., 1997. Drop formation in viscous flows at a vertical capillary tube. Phys. Fluids 9, 2234–2242.

10. Zhang, X., 1999. Dynamics of growth and breakup of viscous pendant drops into air. J. Colloid Interface Sci. 212, 107–122.

11. Sartorelli, J.C., Goncalves, W.M., Pinto, R.D., 1994 Crisis and intermittence in a leaky-faucet experiment," Phys. Rev. E 49, 3963 1994.

12. Clanet, C., Lasheras, J.C., 1999. Transition from dripping to jetting. J. Fluid Mech. 383, 307–326.

13. Eggers, J., Dupont, T.F., 1994. Drop formation in a one-dimensional approximation of the Navier–Stokes equation. J. Fluid Mech. 262, 205–221.

14. Hirt, C.W., Nichols, B.D., 1981. Volume of fluid (VOF) method for the dynamics of free boundaries. J. Comput. Phys. 39, 201–225.

15. Pan, Y., Suga, K., 2006. A numerical study on the breakup process of laminar liquid jets into a gas. Phys. Fluids 18 pp. 0521011–0521011.

16. Che, Z., Wong, T.N., Nguyen, N.T., Yap, Y.F., Chai, J.C., 2011. Numerical investigation of upstream pressure fluctuation during growth and breakup of pendant drops. Chem. Eng. Sci. 66, 5293–5300.

17. Chen, A.U., Notz, P.K., Basaran, O.A., 2002. Computational and experimental analysis of pinch-off and scaling. Phys. Rev. Lett. 88, 1745011–17450114.

18. Farvardin, E., and Dolatabadi. A., 2013. Numerical simulation of the breakup of elliptical liquid jet in still air. J. Fluids Eng., 135, 7, pp. 071302-071302.

19. Delteil, J., Vincent, S., Erriguible, A., Subra-Paternault, P., 2011. Numerical investigations in Rayleigh breakup of round liquid jets with VOF method. Comput. Fluids 50, 10–23.

20. Notz, P.K., Chen, A. U., and Basaran, O. A., Satellite drops: Unexpected dynamics and change of scaling during pinch-off. Phys. Fluids 13, 549 (2001).

21. Wilkes, E.D., Philips, S.D., Basaran, O.A., 1999. Computational and experimental analysis of dynamics of drop formation. Phys. Fluids 11, 3577–3598.

22. Yildirim, O.E., Xu, Q., Basaran, O.A., 2005. Analysis of the drop weight method. Phys. Fluids 17, 0621071–06210713.

23. Subramani, H.J., Yeoh, H.K., Suryo, R., Xu, Q., Ambravaneswaran, B., Basaran, O.A., 2006. Simplicity and complexity in a dripping faucet. Phys. Fluids 18, 03210613.

24. Sallam, K.A., Dai, Z., Faeth, G.M., 2002. Liquid breakup at the surface of turbulent round liquid jets in still gases. Int. J. Multiphase Flow, 427–449.

25. Xiao, F., Dianat, M., McGuirk, J.J., 2016. A robust interface method for drop formation and breakup simulation at high density ratio using an extrapolated liquid velocity. Comput. Fluids 136, 402–420.

26. Rivero-Rodríguez, J., Pérez-Saborid, M., 2017. An efficient finite volume method for one-dimensional problems with application to the dynamics of capillary jets. Comput. Fluids 154, 1, 132–141.

27. Day R.F., Hinch, E.J., Lister J. R., 1998. Self-similar capillary pinchoff of an inviscid fluid. Phys. Rev. Lett. 80, 704.

28. Nikolopoulos, N., Nikas, K.-S., Bergeles, G., 2009. A numerical investigation of central binary collision of droplets. Comput. Fluids 38, 1191–1202.

29. Chakraborty, I., Rubio-Rubio, M., Sevilla, A., Gordillo, J.M., 2016. Numerical simulation of axisymmetric drop formation using a coupled level set and volume of
fluid method. Int. J. Multiphase Flow 84, 54–65.

30. Coullet, P., Mahadevan, L., Riera, C.S., 2005. Hydrodynamical models for the chaotic dripping faucet. J. Fluid Mech. 526, 1–17.

31. Castrejón-Pita, J.R., Castrejón-Pita, A.A., Hinch, E.J., Lister, J.R., and Hutchings I.M., 2012. Self-similar breakup of near-inviscid liquids. Phys. Rev. E. 86, 015301 (R).

32. Borthakur, M.P., Biswas, G., Bandyopadhyay, D., 2017. Formation of liquid drops at an orifice and dynamics of pinch-off in liquid jets. Phys. Rev. E. 96, 013115.

33. Ambravaneswaran, B., Subramani, H.J., Philips, S.D. , Basaran, O.A., 2004. Dripping-jetting transitions in a dripping faucet. Phys. Rev. Lett. 93, 0345011-0345014.

34. Davidson, M.R., Cooper-White, J.J., 2006. Pendant drop formation of shear-thinning and yield stress fluids. Appl. Math. Modell. 30, 1392–1405.

35. Brackbill. J., Kothe D., Zemach, C., 1992. A continuum method for modeling surface tension. J. Comput. Phys. 100 335–54.

36. Youngs, D., 1982. Time-dependent multimaterial flow with large fluid distortion. In: Morton, K.W., Baibes, M.J. (Eds.), Numerical Methods for Fluid Dynamics, pp. 273–285.

37. Suñol., F., González-Cinca R., 2015. Liquid jet breakup and subsequent droplet dynamics under normal gravity and in microgravity conditions. Phys. Fluids 27 (7), 077102.

38. Becker, E., Hiller, W.J., Kowalewski, T.A., 1991. Experimental and theoretical investigation of large-amplitude oscillations of liquid droplets. J. Fluid Mech. 231, 189–210.

39. Rubio-Rubio, M., Taconet, P., Sevilla, A., 2018. Dripping dynamics and transitions at high Bond numbers. Int. J. Multiphase Flow, 104, 206–213.